

# We are IntechOpen, the world's leading publisher of Open Access books Built by scientists, for scientists

6,900

Open access books available

186,000

International authors and editors

200M

Downloads

Our authors are among the

154

Countries delivered to

TOP 1%

most cited scientists

12.2%

Contributors from top 500 universities



WEB OF SCIENCE™

Selection of our books indexed in the Book Citation Index  
in Web of Science™ Core Collection (BKCI)

Interested in publishing with us?  
Contact [book.department@intechopen.com](mailto:book.department@intechopen.com)

Numbers displayed above are based on latest data collected.  
For more information visit [www.intechopen.com](http://www.intechopen.com)



# Laser Welding of Thin Sheet Magnesium Alloys

Mahadzir Ishak<sup>1</sup>, Kazuhiko Yamasaki<sup>2</sup> and Katsuhiro Maekawa<sup>2</sup>

<sup>1</sup>Universiti Malaysia Pahang

<sup>2</sup>Ibaraki University

<sup>1</sup>Malaysia

<sup>2</sup>Japan

## 1. Introduction

Magnesium and its alloys are active materials, and the oxide can easily form when they react with air and moisture (Czerwinski 2002). In addition, magnesium and its alloys are flammable and require strict safeguards during the manufacturing process. These disadvantages make the processing of magnesium alloys into finished products more challenging. These drawbacks cause defects such as cracks, oxide inclusion, burn-through and voids both during and after processing. In order to minimize these defects, most processing methods must be performed at a certain temperature, unlike aluminum alloys and steels, which may be finished by cold working. Defect reduction can be achieved by minimizing the complexity of parts and the number of components produced. Furthermore, improved design techniques and production processing can eliminate defects in the finished products.

In order to produce finished products from several components, welding is unavoidable. However, welding magnesium alloys, especially thin sheets with thicknesses of less than 1.0 mm, is difficult. Furthermore, for electronics and communication devices, the weld width should be as small as possible. Possible methods of welding magnesium alloys include:

- Spot welding
- Arc welding
- Friction stir welding
- Laser welding

The first two methods are suitable for joining thick plates but not very thin sheets, because of the high heat input. Friction stir welding can join thin sheets, but it is difficult to weld complex parts and produces a small weld width. The most versatile and promising process for the fabrication of magnesium parts for electronics parts is laser welding.

The key advantage of laser welding is the ability to narrowly focus the laser beam on a small area, generating high intensity heat without any physical contact between welding hardware and the workpiece. The small area of the heat source can be rapidly scanned along the joint to be welded, and a narrow weld width can be obtained. Other advantages of laser welding include ease of automation and flexibility. Laser welding can be used with three-dimensional components and through transparent heat resistant glass in a vacuum or with

inert gas in a closed box where the introduction of electrodes or tools is impossible. This flexibility can bring new possibilities for joint design and especially for components or parts that feature inaccessible surfaces.

Distortion and deformation of the thin sheet can be significantly reduced by laser welding because of its smaller spot size, lower heat input and improved penetration. These advantages lead to a narrow heat-affected zone (HAZ), which can limit thermal distortion and improve the metallurgical properties compared with arc welding methods. Besides, contamination from electrode materials can be eliminated, and the reduction of volatile alloy components such as zinc can be achieved (Duley 1999).

Currently two main laser systems are used in industry when laser welding sheet metals, namely the pulsed neodymium: yttrium garnet (Nd:YAG) laser and the carbon dioxide (CO<sub>2</sub>) laser.

### 1.1 Types of lasers for magnesium welding

There are only two types of high power laser systems that are currently available for industrial use that are suitable for welding. These lasers are carbon dioxide (CO<sub>2</sub>) and neodymium: yttrium garnet (Nd:YAG) lasers.

#### 1.1.1 Neodymium: Yttrium Aluminum Garnet (Nd:YAG) laser

The active medium in the Nd:YAG laser is a solid crystal material of yttrium aluminum garnet (YAG) doped with neodymium ions, Nd<sup>3+</sup>. The neodymium ions take the position of the yttrium ions in the garnet lattice in which they are roughly the same size. The ion concentration is around 1.0% by weight (Ion 2005). Neodymium: yttrium aluminum garnet (Nd:Y<sub>3</sub>Al<sub>5</sub>O<sub>12</sub>) is a solid structure that is used as a lasing medium for a solid-state laser.

This crystal produces infrared light with a wavelength of 1.06 μm. In addition, wavelengths of 940, 1120, 1320 and 1440 nm can be generated. One of the advantages of this laser is that its lower wavelength gives better absorption by metals. The other advantage is that it allows the use of an optical fiber to transfer the laser beam to a certain distance. The standard power outputs are 0.3- 3 kW, but advances in this laser can extend the maximum power available to 4.0 kW. This laser may be operated in continuous and pulsed modes.

#### 1.1.2 Carbon dioxide (CO<sub>2</sub>) laser

The CO<sub>2</sub> laser (carbon dioxide laser) is a laser based on a gas mixture as the gain medium, which contains carbon dioxide (CO<sub>2</sub>), helium (He) and nitrogen (N<sub>2</sub>). This laser is electrically pumped via a gas discharge, which can be operated with DC current, AC current (e.g. 20-50 kHz) or in the radio frequency (RF) domain. Nitrogen molecules are excited by the discharge into a vibration level and transfer their excitation energy to the CO<sub>2</sub> molecules when colliding with them. Helium serves to reduce the lower laser level and to remove the heat. Other constituents such as hydrogen or water vapor serve (particularly in sealed-tube lasers) to re-oxidize carbon monoxide (formed in the discharge) to carbon dioxide.

This laser produces infrared light with wavelengths from 9.6 μm to 10.6 μm. CO<sub>2</sub> lasers are usually used in industrial applications. Its output power is up to 50 kW, and the system is

simple and reliable. The output efficiency defined as the ratio of output laser power to input electrical power can reach up to 10 %, which is efficient. However, it cannot be transferred via fiber optics.

### 1.1.3 Selection of laser source for welding magnesium alloys

Laser welding of metal in many industries uses both CO<sub>2</sub> and pulsed Nd:YAG lasers (Costaa, Quintinoa et al. 2003; Haferkamp, Ostendorf et al. 2003). Both lasers have unique advantages. However, one of the leading advantages of the Nd:YAG laser over the CO<sub>2</sub> laser in this specific application is the that lower wavelength gives better absorption by metals. However, the continuous mode of Nd:YAG possesses less power, which results in low power density. Thus, the laser usually is used in pulsed mode to raise the power and increase the power density.

The thicknesses of the metal welded in previous studies were mostly above 1.0 mm (Costaa, Quintinoa et al. 2003; Haferkamp, Ostendorf et al. 2003; Quan, Chen et al. 2008). The research on welding thin sheets of magnesium alloys lower than 1.0 mm is still deficient. Therefore, in this study, the pulsed Nd:YAG laser is chosen to weld thin sheets of magnesium alloy with thicknesses of 0.3 mm.

## 2. Nd:YAG laser system for welding magnesium alloys

### 2.1 Principles of the laser system

The laser that is used in this study is a pulsed Nd:YAG laser. The schematic of the laser optical system is shown in Fig. 2.1. It is a solid state laser in which the rod-shaped laser crystal is illuminated with visible light. The source of the energy is a plasma flash lamp (electrical discharge in a quartz tube filled with inert gas. The laser rod stores the pumping light energy for a short time at the pumped electron levels. The energy is emitted once again as infra red light with a wavelength of 1064 nm.

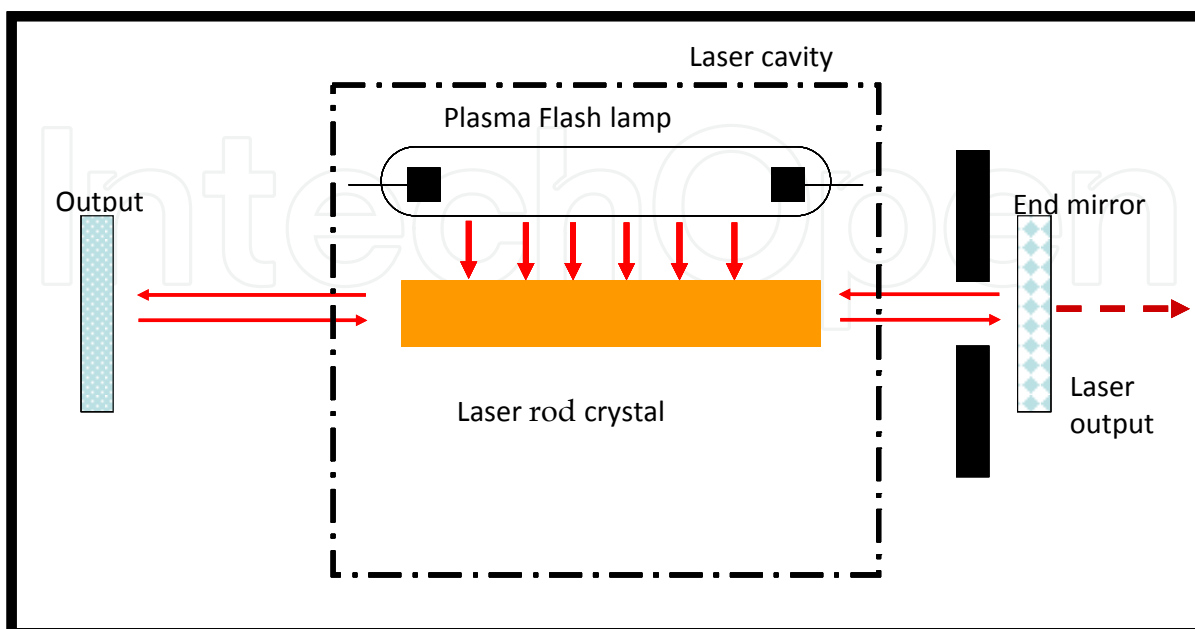


Fig. 2.1. Schematic illustration of Nd:YAG laser cavity

The optical resonator includes the laser crystal and two parallel mirrors, which enables multiple passages through the crystal. This can lead to induced light emission and therefore to coherent light. The laser radiation emerges through the partially reflecting out-coupling mirror.

## 2.2 Characteristic of the laser beam

The advantage of lasers compared with other powerful sources of light is their ability to concentrate beam energy onto a very small area, called the focus point. The distribution of the intensity in the application is another quality parameter. In this study the beam energy intensity is single mode, which results in a near-Gaussian distribution.

## 3. Laser parameters

The main parameter for a pulsed laser is the pulse energy,  $E$ , which can be adjusted by controlling the pulse duration, repetition rate and voltage. Other parameters such as the peak power and average power can be determined by the following equations.

$$P_p = \frac{E}{P_{avg}} \quad (3.1)$$

$$P_{avg} = E \times rep.rate \quad (3.2)$$

$P_p$ ,  $E$ ,  $P_{avg}$  and  $rep.rate$  are the peak power, pulse energy, average power and repetition rate, respectively.

### 3.1 Laser material interactions

When a laser beam impacts a material, certain portions of the beam energy are reflected, absorbed and transmitted. The relation between the reflection  $R$ , absorption  $A$  and transmission  $T$  is as follow.

$$R + A + T = 1 \quad (3.3)$$

However, when a laser beam impacts a flat sheet of metal, a large portion of the energy is reflected, a small portion is absorbed, and no transmission occurs. Transmission usually only occurs for transparent materials such as glass, polymers, etc. When a flat metal is used, the reflected energy is lost to the environment. The remaining energy is absorbed in the metal as heat, which raises the temperature of the material under the beam and is conducted into the bulk of the material. Thus, for a metal surface the relation between  $R$  and absorption is:

$$R + A = 1 \quad (3.4)$$

The reflection percentage can be measured using a power detector. The reflection ratings of some metals, including the AZ31B alloy, are shown in Fig 3.1. It is apparent from the figure that the reflection of wrought AZ31B sheet metal with a thickness of 1.3 mm is 94 %. The reflection metric decreases to around 88% when the surface of the sheet metal is polished with SiC paper (#1000). Coating the sheet metal surface with silver nanopaste significantly reduces the reflection to around 36%. It is probable that the roughness and the coating

material cause the decrease in the reflection and the increase in absorption. The absorptivity may be enhanced by many factors such as temperature, surface roughness, oxidation and changes in morphology (Duley 1998).

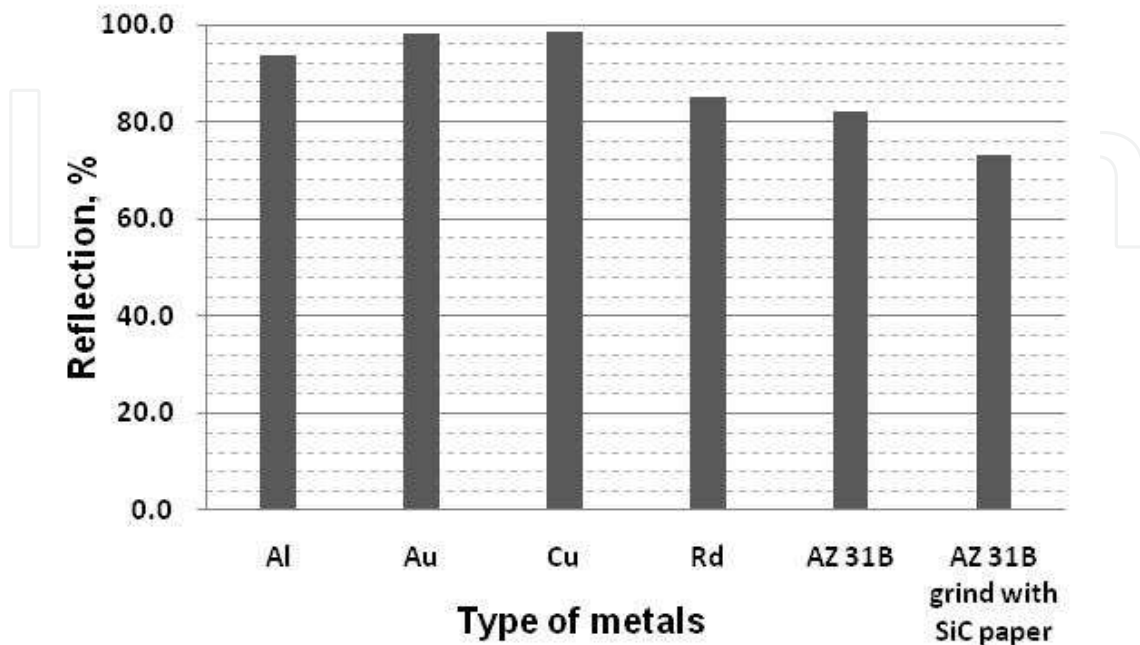


Fig. 3.1. Laser reflections of different materials (Ishak 2010)

### 3.2 Laser welding characteristics

Conduction mode welding occurs at a low energy density and involves the laser beam interacting with the surface of the sheet metal. The energy is absorbed by the atoms on the metal surface, which heat up and then transfer the heat to the atoms below the surface. Typically, conduction mode welding is useful when the energy density is relatively low. The process generates a wide weld bead. The cross-sections of conduction mode welds exhibit wide beads and relatively shallow depths. The size and shape of the weld bead depends upon the input energy and the material properties.

At high heat energy density, the metal surface rapidly heats up to the point where molten metal vaporizes at the center of the weld beam spot, which opens up a blind cavity (keyhole) in the molten metal. As the keyhole penetrates deeper into the metal, the laser light is scattered repeatedly within it, thus increasing the coupling of the laser energy to the workpiece. While the laser energy is applied, the keyhole is held open by vapor pressure, which prevents the keyhole wall from collapsing. A higher penetration depth and a narrower weld bead can be achieved with the keyhole mode.

### 3.3 Difficulties in laser welding of magnesium and its alloy thin sheet

The basic difference between the conduction mode and penetration mode is that the surface of the weld pool remains unbroken during conduction mode welding. The opening of the surface allows the laser beam to enter the melt pool in the keyhole mode and causes a break in the metal surface. In addition, openings in the molten metal result in gas entrapment during welding, which leads to the formation of pores in the weld.

The high intensity of the energy density in the keyhole mode can penetrate thicker metal compared with the conduction mode; however, to weld thin metal sheets the keyhole mode can cause cut or blow holes in the metal to be joined. Low heat input generates less distortion, and lower thermal distortion occurs with the conduction mode than with the keyhole mode. Based on these reasons the conduction mode is preferable to weld thin sheet magnesium alloy with thicknesses of 0.3 mm.

#### 4. Bead on plate welding

The aim of bead on plate welding experiment is to study the laser welding properties of AZ31B magnesium-based sheet. Effects of welding parameters such as pulse energy, focal position, and scan speed on weld appearances were extensively investigated. This study could provide basic information regarding the laser parameters and weld appearances prior to lap fillet configurations.

##### 4.1 Experimental method

The AZ31B magnesium-based sheet with a thickness of 0.6 mm was studied in this experiment. The sheets were cut into 20 x 30 mm specimens. Prior welding, the specimens were polished with SiC paper and cleaned using ethanol to remove oil film that existed on the material surface. In this study bead on plate welding was carried out.

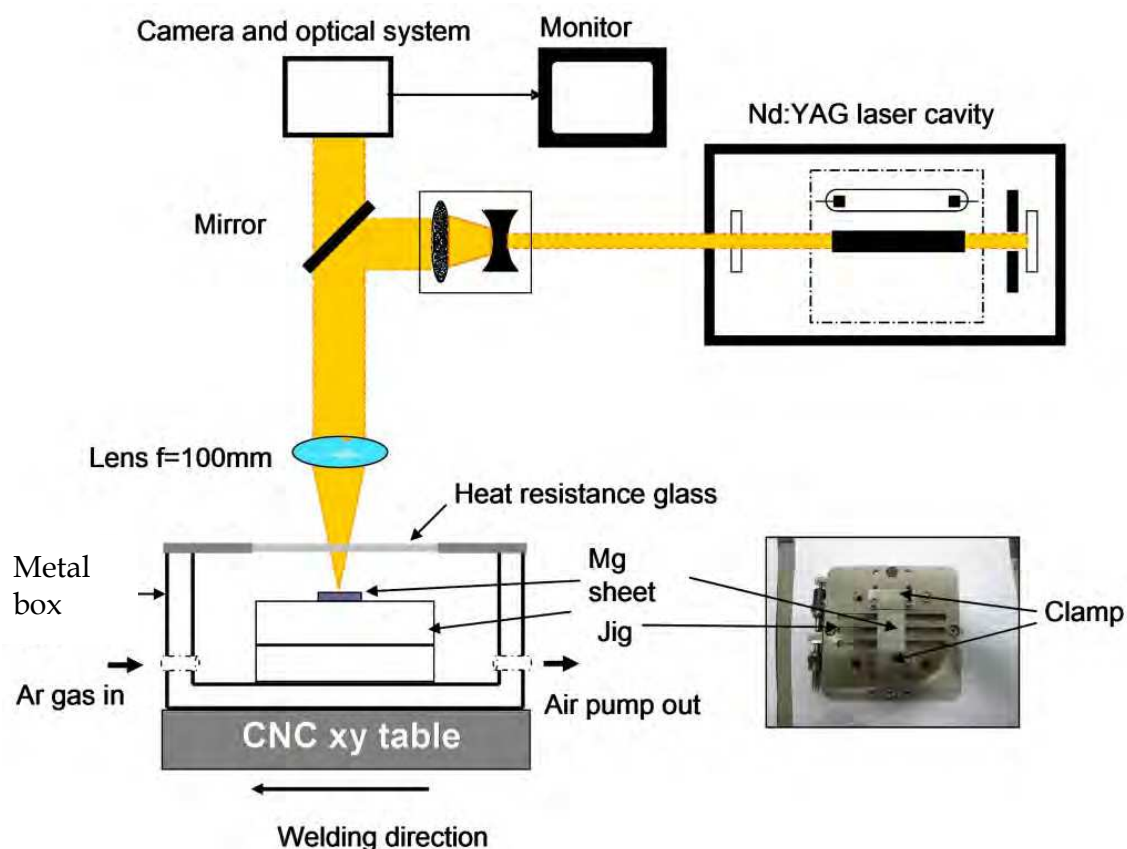


Fig. 4.1. Laser system and experimental set-up for bead on plate welding

A pulsed Nd:YAG laser with 1.06  $\mu\text{m}$  wavelength and 100 mm focal length was used in this investigation. Spot size of a focused laser beam was measured about 0.4 mm. Fig. 4.1 illustrates the set-up for the bead on plate welding. The sheet was fixed on special jigs by clamping. The jig with a sheet was placed in a steel box having the top of the box was partially closed by a heat-resistant glass, where the laser beam is transmitted through the glass during welding. Argon gas was filled in for about 30 s as a shielding gas to prevent oxidation prior to welding, and gas flow was continued until welding finished. During the welding process, the laser beam was kept stationary while steel box was moved with a CNC x-y table. The laser beam was transverse the specimen surface, as shown in Fig.4.1.

The parameters used were laser pulse energy in the range of 1.0 J to 2.5 J, welding speed between 50 mm/min to 600 mm/min and beam defocusing in the range of -4.0 mm to +4.0 mm. Positive defocusing is defined as that the focal point above the top surface of specimen whereas negative one the focal point below the top surface. The repetition rate and pulse duration were constant at 80 Hz and 3.0 ms, respectively. After welding, the sample was cut into four parts, being mounted in a polymer resin. The cross-section was etched with an etchant (10 ml acetic acid diluted with 100 ml distilled water) for macroscopic observation. The penetration depth, bead width and undercut depth of the weld were measured by optical microscopy.

## 4.2 Results and discussions

### 4.2.1 Effect of focus point position

Fig. 4.2 shows the cross-sectioned appearance of bead on plate welding. By irradiating laser beam, many layers were formed from molten magnesium. The wider bead with shallow penetration depth shows that the type of welding is conduction mode welding rather than keyhole mode welding; conduction mode welding is resulted because of low energy density. Figure 4.3 shows the relationship between the focus position effect and penetration depth. The ranges can be varied from -4.0 mm to 3.0 mm in using this laser system. The focal point located just on the specimen surface produced the lowest depth. Increase or decrease in focus point location gradually increases the penetration depth. The highest depth penetration was achieved when the focus position is at a defocus point of -3.0 mm. (Zhu, Li

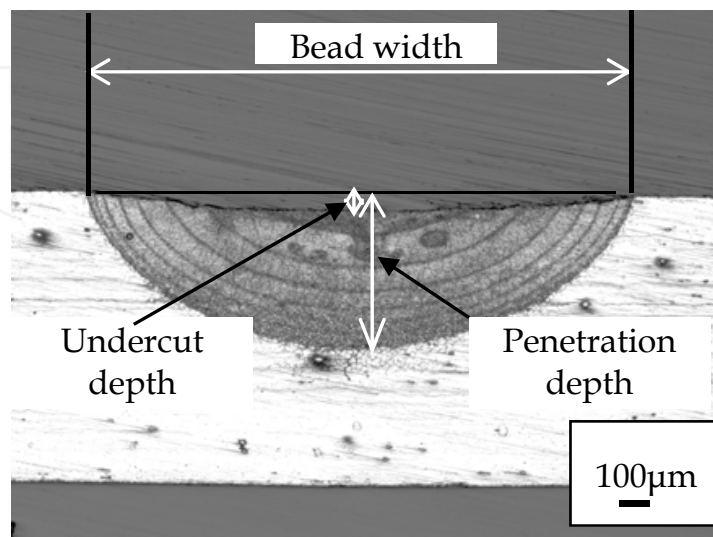


Fig. 4.2. Bead on plate weld appearance

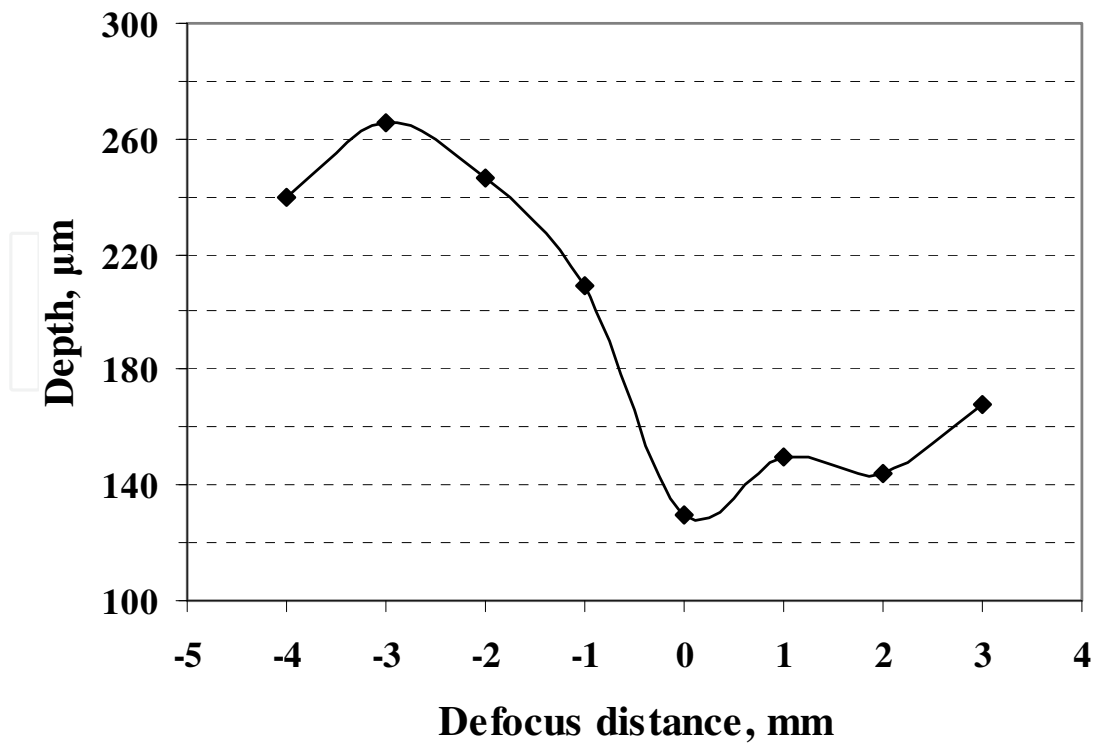


Fig. 4.3. Defocus effect on penetration depth

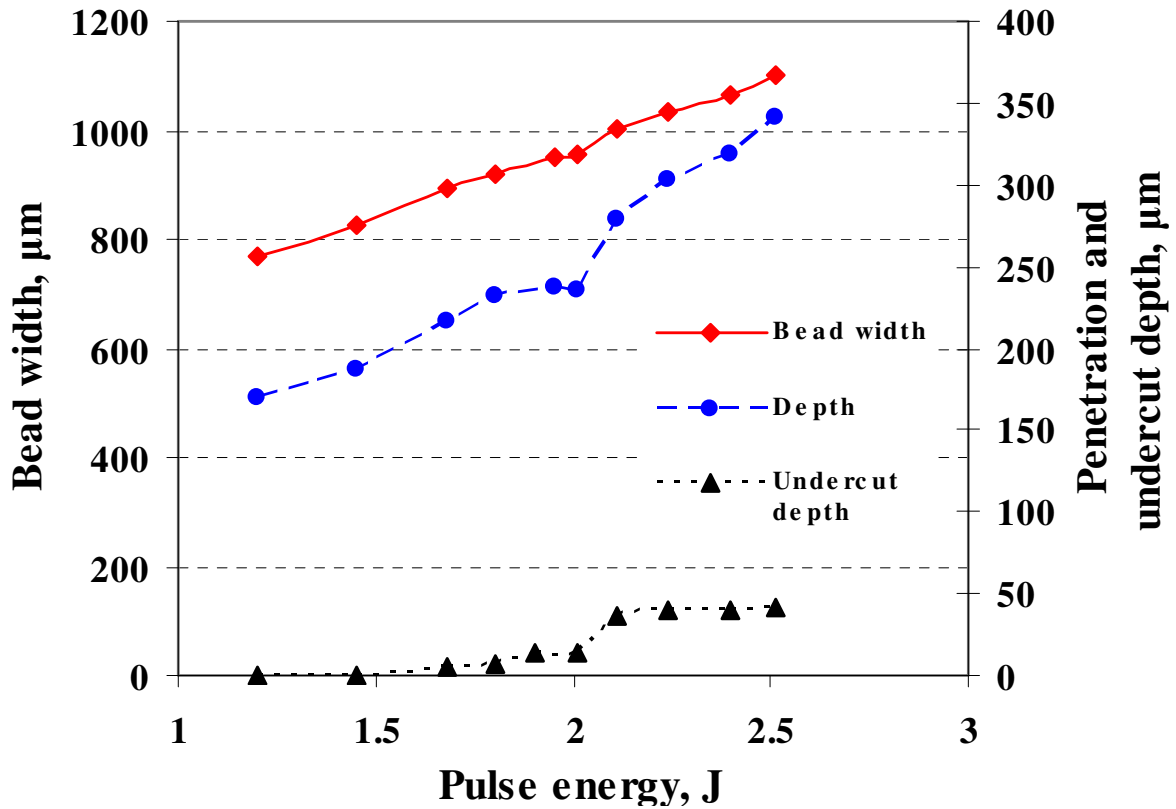


Fig. 4.4. Pulse energy effect on bead width, penetration and undercut depth

et al. 2005) reported that using CO<sub>2</sub> laser welding even at low power undercut occurs and can be avoided by defocusing. On the contrary, our results show that using Nd:YAG laser welding with different defocusing positions produced no effect on undercut. Thus, the defocus point at -3.0 mm was used throughout the investigation because it generated the maximum penetration depth.

#### 4.2.2 Effect of pulse energy

Fig. 4.4 shows the effect of laser pulse energy on weld bead width, penetration depth and undercut depth when the scan speed was 300 mm/min. It is observed that the weld width becomes obviously larger when high pulse energy is used.

This indicates that the size of weld pool is increased with increasing pulse energy. There was no weld appearance observed when pulse energy was below than 1.2 J. Which mean that in this case, the threshold pulse energy of laser welding is about 1.2 J. Increase in pulse energy also resulted in deeper penetration depth; however, full penetration was not achieved for the 0.6 mm thickness specimen.

#### 4.2.3 Effect of scanning speed

The weld bead width and penetration depth under different welding speeds with constant pulse energy of 1.8 J are depicted in Fig. 4.5. It is shown that the bead width and penetration depth increase when welding speed decreases. This result is consistent with the effect of laser pulse energy as was shown in Fig. 4.4. However, increase in pulse energy causes

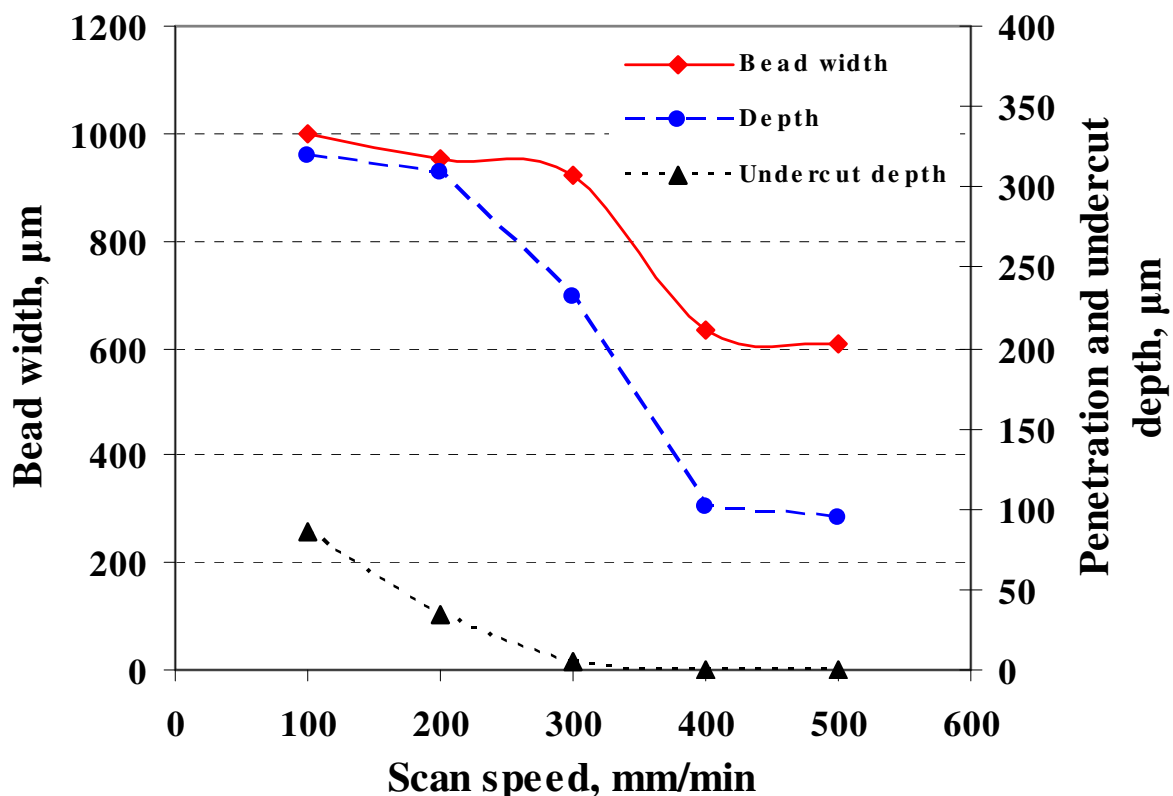


Fig. 4.5. Scan speed effect vs. width, penetration depth and undercut depth

deeper undercut depth. The same condition occurred when welding speed decreases, as shown in Fig. 4.5. When higher pulse energy or lower welding speed is used, the heat input per unit length will increase as equation 4.1.

$$E = \frac{E_p \times f}{v \times d_o} \quad (4.1)$$

Where,  $E_p$ =pulse energy (J),  $f$ =rep. rate (Hz),  $v$ =scan speed (m/min) and  $d_o$ =beam diameter. Higher heat input leads to more molten metal and large weld width. Higher heat input could evaporate more molten metal from the surface, so that undercut takes place.

#### 4.2.4 Weld appearances and defects

Full penetration is more suitable for laser welding, but it was not achieved either by increase the pulse energy or low speed weld for this specimen thickness, 0.6 mm. When welding was carried out, scan speeds lower than 100 mm/min with pulse energy of 1.8 J, burn through took place especially at both edges of specimen and the weld appearance was very bad as shown in Fig. 4.6. The phenomenon was observed when higher pulse energy was over than 2.5 J at a welding speed 300 mm/min. The major concerns for welding magnesium alloys are the formation of cracks and pores. These defects could lead to low strength in welded products. As shown in table 4.1, a long crack was observed at scan speeds of 100 mm/min to 200 mm/min. At a scan speed of 50 mm/min, burn through occurred at both edges of the specimen together with a long crack presence at the middle of weld bead. Cracks appear at a scan speed 100 mm/min as shown in Fig. 4.7(a), where they exist at the center of weld bead or in the fusion zone and relatively was long. The crack length reduces as scan speed increase to 200 mm/min, and then no macro cracks were observed when the scan speed was further increased from 300 mm/min to 500 mm/min. A lot of pores were observed in every scan speed when the weld was formed at constant pulse energy 1.8 J. Figure 4.8 shows the appearances of pores when weld at different scan speeds. The number of pores was reduced at 200 mm/min and 400 mm/min, where as many a lot of pores can be observed at a scan speed 300 mm/min. The remaining pores may be originated mainly from initial preexisting pores in the sheet. The growth of pores could result from the expansion and coalescence of the remaining pores, which produces larger pores in the weld bead. The pores formed during the first run of welding could be reduced by well controlled second run of welding (Zhao and Debroy 2001).

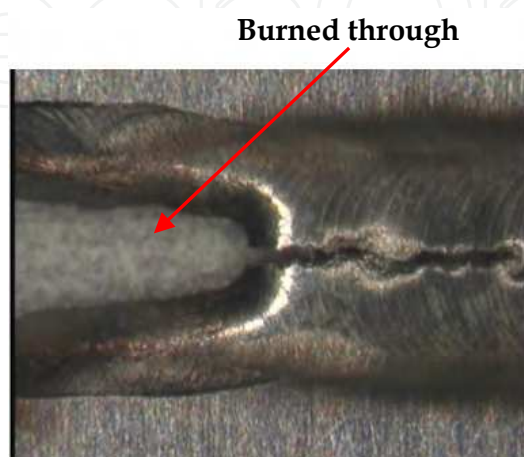


Fig. 4.6. Burned through and cracks at scan speed 50 mm/min

Scan speed (mm/min)	50	100	200	300	400	500	600
Weld condition	Burn through and long crack	Long crack	Cracks	Good	Good	Good	No bead

Table 4.1 Weld condition after welding with pulse energy 1.8 J at different scan speed

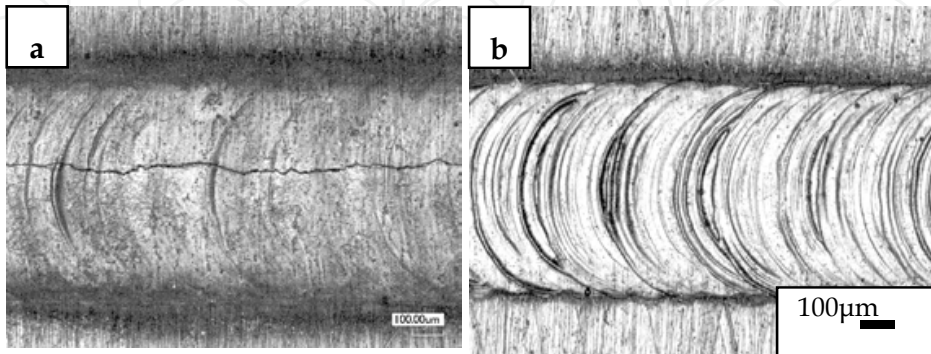


Fig. 4.7. Top view of bead scan speed a) 100 mm/min and b) 300 mm/min.

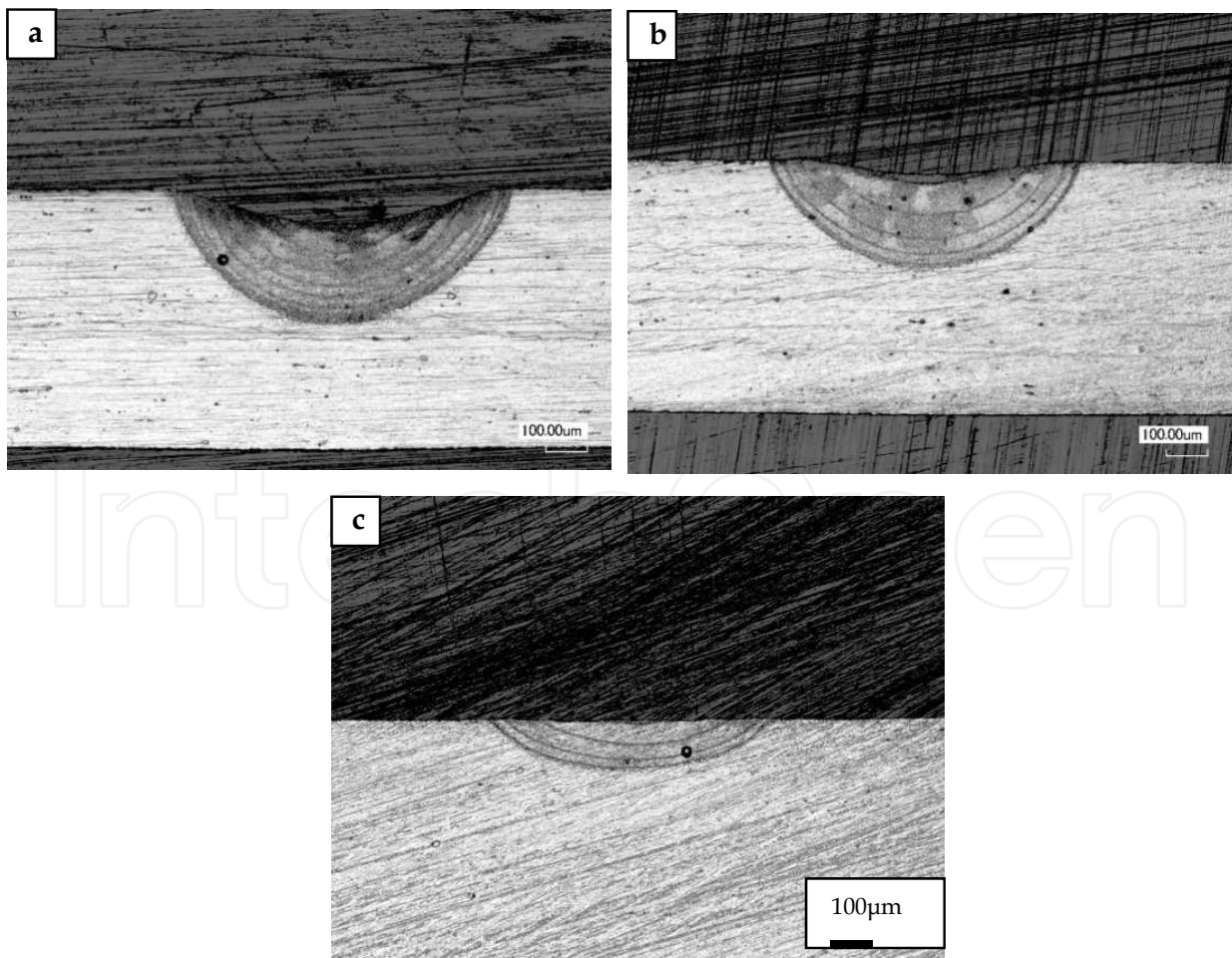


Fig. 4.8. Pores at scan speeds of a) 200 mm/min, b) 300 mm/min and c) 400 mm/min

## 5. Fillet welding of AZ31B magnesium alloy thin sheet

The welding of thin sheets is usually more problematic than welding thick sheet metal. Such problems are usually related to the high heat input of conventional arc welding processes. This high heat input leads to various problems such as cutting, burn through, distortion, porosity, cracking, etc. Thus, the selection of an appropriate welding process, procedure and technique are important in order to prevent these problems. Compared with arc welding, laser welding and electron beam welding are excellent methods that offer many advantages, such as narrow welds and impressive penetration depths. However, laser beam welding is the best choice because it can be used at ambient pressures and temperatures. However, the laser welding of thin sheet metals can still be problematic. Issues include the loss of material due to evaporation and inadequate control of heat, which leads to cutting and melt-through issues (Aghios, Bronfio et al. 2001; Cao, Jahazi et al. 2006; G. Ben-Hamu 2007). There are plenty of reports on the welding of copper, stainless steel and aluminum alloys (Aghios, Bronfio et al. 2001; Cao, Jahazi et al. 2006; G. Ben-Hamu 2007) in thin sheets of less than 1 mm thickness, but few studies have been published to date that focus on thin sheets of similar thickness in the case of magnesium alloys.

This chapter focuses on a Nd:YAG laser that was utilized to lap fillet weld AZ31B magnesium alloys thin sheet. The rationale behind the selection of AZ31B magnesium alloys focused on its unique properties. Magnesium alloys have a low density, high strength-to-weight ratio, high damping capacity and good recyclability; they have recently attracted more attention in many industries (Liming Liu and Changfu Dong 2006). However, processing magnesium alloys can be difficult due to defects such as cracks, pores and cuts (Ukita, Akamatsu et al. 1993; Leong, Sabo et al. 1999; Moon Jonghyun 2002; Toshikatsu Asahina 2005; Zhu, Li et al. 2005). This research focuses on the power density of the laser beam in conduction-mode welding applications, which results in a very stable weld pool. The absence of unstable fluid motion, which is usually present in keyhole mode welding, can lead to attractive weld qualities as well as good control of penetration depths. The advantages of conduction mode welding make it much more suitable for welding thin magnesium alloy sheets as thin as 0.3 mm.

### 5.1 Experimental

#### 5.1.1 Material

Lap fillet welding by laser was performed on a 0.3 mm thickness of magnesium alloy sheet of AZ31B. The size of the sheet was 20 mm x 30 mm. Before welding, the sheets were polished with SiC paper and then cleaned with ethanol to remove oxide films, oil and dirt.

#### 5.1.2 Nd:YAG laser

A pulsed Nd:YAG laser with a 1.06  $\mu\text{m}$  wavelength, 0.4 mm beam spot diameter and 100 mm focal length lens were used for this experiment.

#### 5.1.3 Experimental set-up

Figure 5.1 illustrates the set-up for the lap fillet welding experiment. Lap welding was performed by overlapping the two sheets, which were then joined by a laser at the edge side

of the upper sheet. The distance between the clamps was 4 mm, and the edge of the upper sheet was equidistant from the two clamp arms. A specimen was fixed with jigs in a steel box and then located on a CNC X-Y table. The top of the box was partially closed by a heat resistant glass, through which the laser beam was transmitted during welding. Prior to welding, argon gas was pumped into the box at a flow rate of 20 L/min to prevent oxidation and continued flowing until the welding was finished.

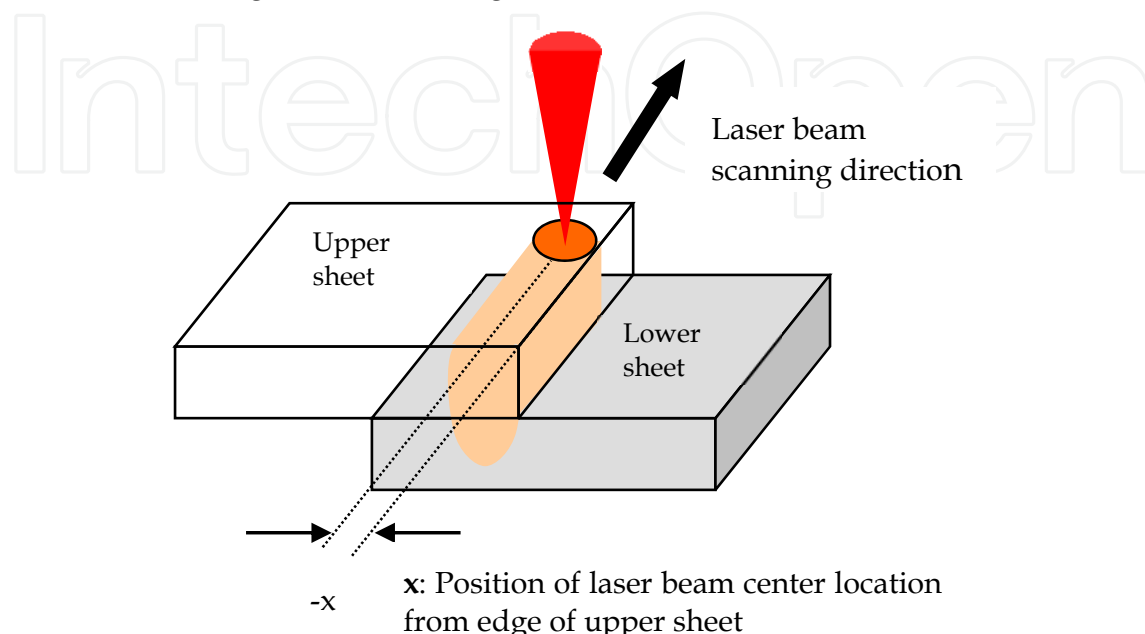


Fig. 5.1. Beam center location from edge of upper sheet (Ishak, Yamasaki et al. 2009)

#### 5.1.4 Laser welding parameters

In this experiment, the two sheets were welded with different values of gap width from 0 to 100  $\mu\text{m}$ , and the beam center located on the edge of the upper specimen ( $x=0$ ). Next, the laser beam center location ( $x$ ) was varied from the edge of the upper sheet towards the  $-x$  direction, as shown in Fig. 5.1: -0.1, 0, 0.1, 0.2 and 0.3 mm with varying scan speeds from 50 to 600 mm/min. The setting of the laser beam on a specific location on the upper sheet was determined by a camera using the precisely controllable CNC table to an accuracy of 1  $\mu\text{m}$ .

As concluded from the bead on plate study described in section 4, defects such as undercuts, cracks and pores can be reduced by proper control of laser parameters such as the pulse energy and pulse duration. Therefore, the parameters for Nd:YAG laser welding such as pulse energy, pulse duration and repetition rate were fixed at 1.8 J, 3.0 ms and 80 Hz, respectively. The laser beam was scanned in the  $y$  direction during welding.

## 5.2 Results and discussions

### 5.2.1 Effect of gap size on weld geometry

The effect of the gap width between the two sheets on the weld appearance was investigated. Lap fillet welding was carried out at beam location  $x=0$  with varying gap

width. The laser parameters of pulse energy, pulse duration and scan speed remained constant at 1.8 J, 3.0 ms and 350 mm/min, respectively. The gap width and resulting welds are shown in Fig.5.2. An increase in the gap width to 35-55  $\mu\text{m}$  generates a wide void, and further increase of the gap to 55-80  $\mu\text{m}$  produces a wider and larger void. Gap widths of less than 35  $\mu\text{m}$  significantly reduce the size and create a round shape void.

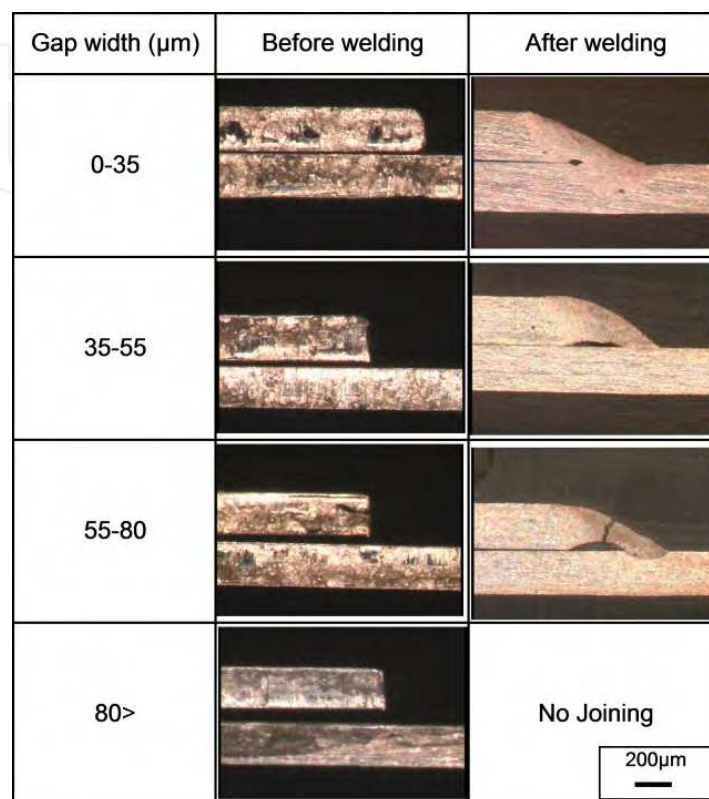


Fig. 5.2. Gap width effect on weld appearances at beam location  $x=0$  (Ishak, Yamasaki et al. 2009)

Wider gaps over than 80  $\mu\text{m}$  fail to create a joint. A gap wider than about 35-55  $\mu\text{m}$  creates a long crack that starts at root of the two sheets. The crack then expands to the upper surface of the weld bead. Additionally, when the gap width exceeds 35  $\mu\text{m}$ , the amount of molten metal is insufficient, and thus the bond width and penetration depth become small. These results suggest that the gap width is the most important factor in the occurrence of defects as well as in controlling the bond width and penetration depth of thin sheets. Therefore, to minimize the defects and optimize the bond width and penetration depth, the gap width must be restricted to less than 35  $\mu\text{m}$ .

### 5.2.2 Effect of laser beam center position on weld geometry

To analyze the weld geometry of the sample, the average weld width and penetration depth were measured. The effects of the center beam location on the bond width and penetration depth are shown in Figs.5.3 and 5.4. The weld bond width and penetration depth decreased significantly with increasing distance of the beam center location from the edge of the upper specimen. The weld bond width and penetration depth decreased significantly with increasing distance of the beam center from the edge of the upper specimen. A larger

distance results in a low heat concentration on the upper surface of the specimen. This occurs due to heat being dissipated to the surroundings because the magnesium alloy exhibits high thermal conductivity. Less heat is absorbed by the workpiece, resulting in a smaller melted weld area. An increased distance may also increase the size of voids at the root, as shown in Fig. 5.2. From this result, we conclude that the weld geometry in laser welding is very sensitive to beam center location distances on the order of 100  $\mu\text{m}$ .

### 5.2.3 Microstructure

Figure 5.5 shows the weld microstructure obtained at  $x=0$  with scan speeds of 250, 350 and 450 mm/min. Table 5.1 lists the mean grain size with different scan speeds and locations. Fine grains are apparent at the upper weld with an average grain size of  $3.5 \mu\text{m}^2 \pm 2.3$  for the 450 mm/min scenario. A mix of fine and medium-large grains with an average grain size of  $17 \mu\text{m}^2 \pm 11$  can be seen at the middle of weld bead, given a joint between the two sheets. These grain sizes are much smaller than those reported elsewhere, where grain sizes were as large as 20  $\mu\text{m}$  in the fusion zone (Cao, M.Jahazi et al. 2006; Y.Quan 2008).

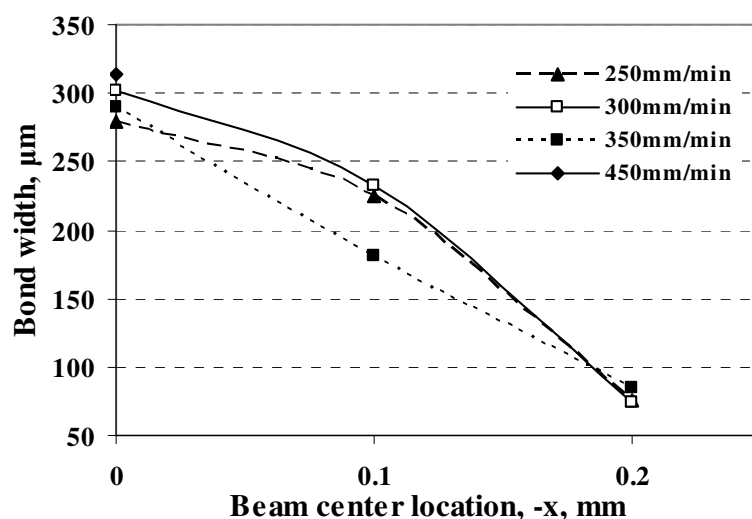


Fig. 5.3. Bond width at different beam location

Large elongated grains with an average grain size of  $141 \mu\text{m} \pm 89$  are apparent in region III, and non-uniform shapes with an average grain size of  $13.5 \mu\text{m} \pm 9.0$  can be seen in region IV. The microstructure at location IV is the same as that of the base metal. There are no significant changes in terms of grain size between scan speeds of 350 mm/min and 450 mm/min at each region.

With a scan speed of 250 mm/min, the average grain size in region I is about  $27 \mu\text{m} \pm 18$ . An increase in the grain size is observed in region II with a grain size of about  $53 \mu\text{m} \pm 31$ . However, we observed no changes in grain size in region III, while in region IV a larger grain size of about  $26 \mu\text{m} \pm 12$  was apparent at the bottom of the weld. The lengths of the long elongated grains decrease as scan speed increases, as listed in table 5.2.

We conclude that the grain size increases with increasing distance from the upper weld because of the changes in thermal cycling during welding. The grain size at the fused area

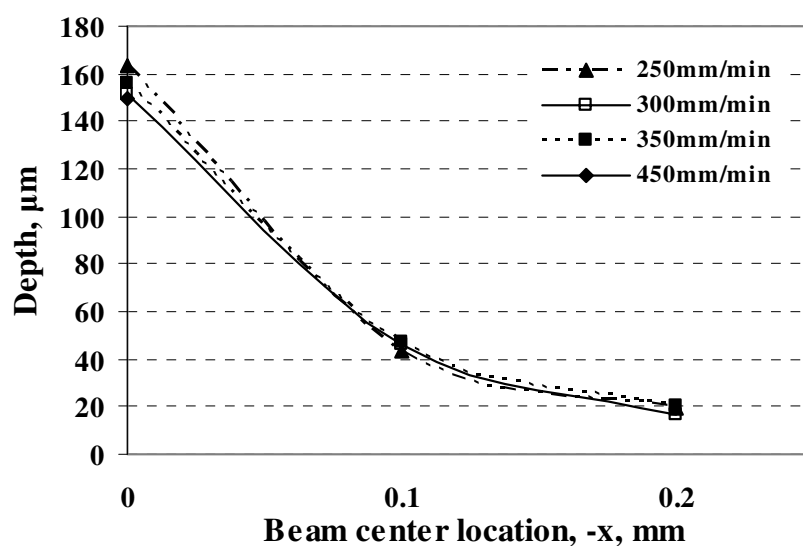


Fig. 5.4. Penetration depth at different beam location

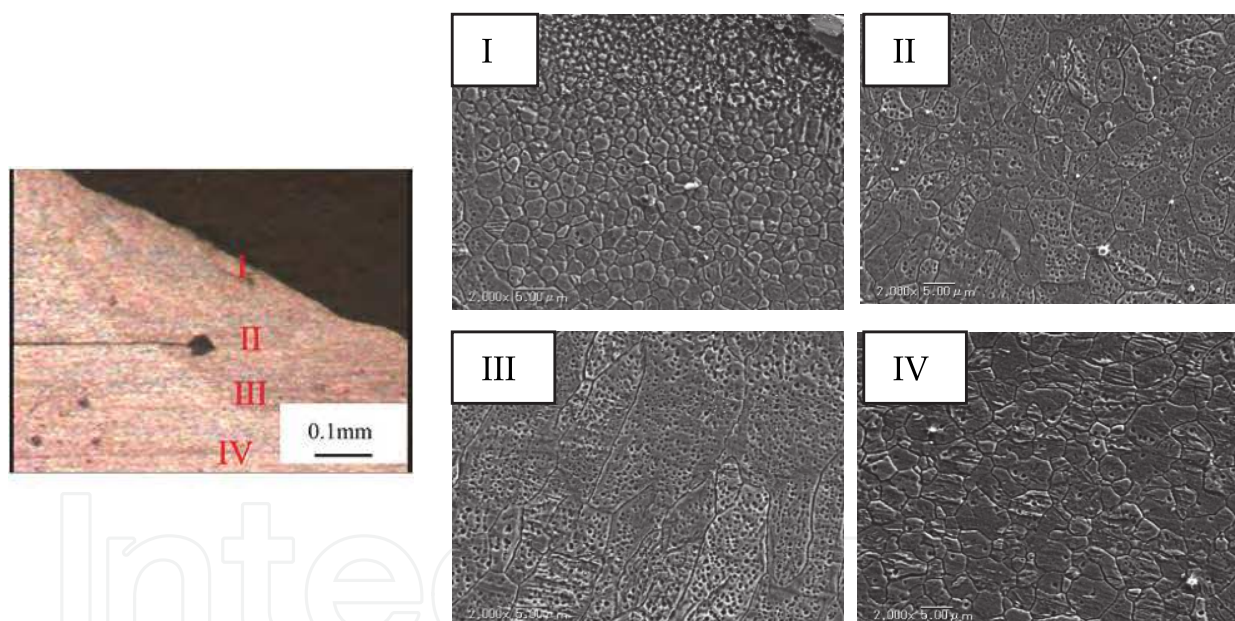


Fig. 5.5. Microstructure of welded joints at scan speed 450 mm/min at four different regions (Ishak, Yamasaki et al. 2009)

Mean grain size, $\mu\text{m}$				
Weld region	I	II	III	IV
250 mm/min	$27 \pm 18$	$53 \pm 31$	$98 \pm 57$	$26 \pm 12$
350 mm/min	$4.0 \pm 1.5$	$18 \pm 15$	$160 \pm 84$	$14 \pm 10$
450 mm/min	$3.5 \pm 2.0$	$17 \pm 11$	$141 \pm 89$	$13.5 \pm 9.0$

Table 5.1. Mean grain size at different scan speed and location

becomes larger at lower scan speeds. A low scan speed will result in impaired cooling. Moreover, since the cooling rate during solidification can be small, the time for grain coarsening will become longer. A large number of precipitated particles will also be apparent in the form of a very fine white deposit in the weld area. It has been reported elsewhere that the sole precipitation phase of AZ31 magnesium alloy is  $\gamma$ -Mg<sub>17</sub>Al<sub>12</sub>, and the white particles have been identified as Mg<sub>17</sub>(Al, Zn)<sub>12</sub> (Quan, Chen et al. 2008).

Scan speed , mm/min	250	350	450
HAZ length	187 ± 14 (Area III and IV)	112 ± 8 (Area III)	83 ± 10 Area II

Table 5.2. HAZ length at different scan speed and location

## 5.2.4 Defects

### 5.2.4.1 Void at the root

Void at the root between the two sheets are apparent at almost all beam center locations and scan speeds. An increase in beam location distance makes the void size larger. Larger voids reduce the bond widths of the joints. By contrast, the size of voids can be reduced by selecting a high scan speed. The void size can be greatly reduced to around 0-40  $\mu$ m at a beam location of  $x=0$  and with a scan speed of 400-450 mm/min.

The void or discontinuity at the weld root probably occurred because of a lack of fusion (Yamauchi, Inaba et al. 1982; Nobuyuki, Masahiro et al. 2002; G.Rihar and M.Uran 2006; Z. Barsoum and A. Lundback 2009). This probably happens because of insufficient melting of the lower sheet, although the upper sheet can be heated at the welded root area as shown in Fig. 5.6. This insufficient melting was due to inadequate energy input and weld preparation throughout the welded root area (Yamauchi, Inaba et al. 1982; Nobuyuki, Masahiro et al. 2002; G.Rihar and M.Uran 2006; Z. Barsoum and A. Lundback 2009). The narrow gap may also contribute to a lack of fusion. Furthermore, we believe that an oxide thin film probably formed on the surface of the lower sheet, although it had been polished using SiC paper of grit 1000 and cleaned using acetone. Magnesium is an active metal, and oxide can easily form on the surface when in contact with air after grinding (Z. Barsoum and A. Lundback 2009). This thin layer may have acted as a barrier, preventing heat transfer to the lower sheet.

### 5.2.4.2 Cracks

Cracks are apparent at lower speeds when  $x=0$  and become smaller as the scan speed is increased. No visible cracks were observed at the beam center location  $x=0$  with scan speeds of 400 to 450 mm/min. Furthermore, no macro cracks were observed on the surface of the upper sheet weld bead. The appearance of the cracks proved to be highly consistent across all specimens at low scan speeds. The crack profile indicates that cracking initiated from the root and then propagated into the weld metal but not to the center or upper surface of weld zone. From microstructure images, we conclude that the cracking occurred and propagated in the large grain area in a transgranular manner.

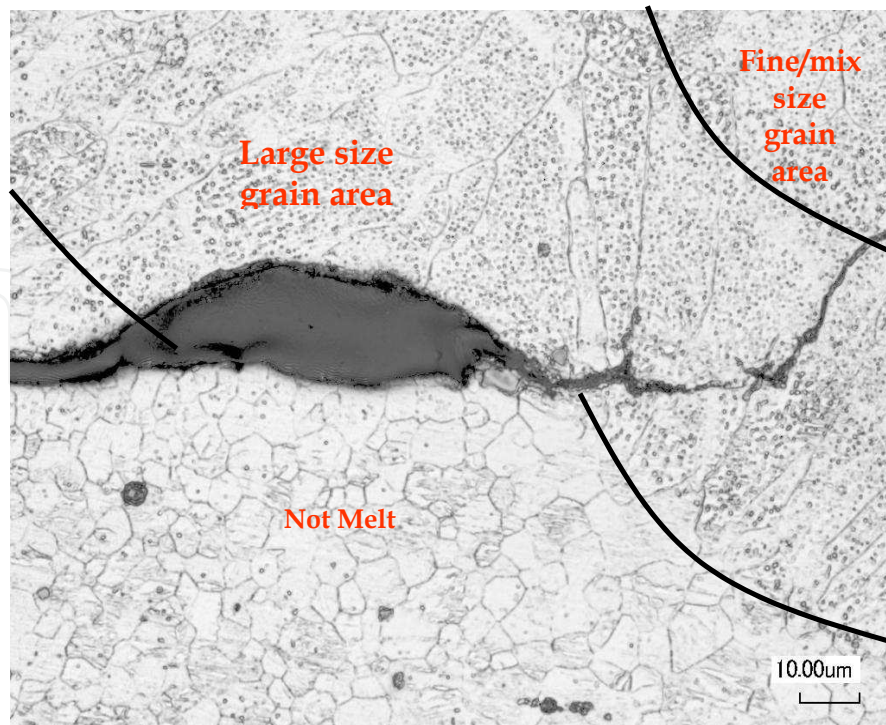


Fig. 5.6. Microstructure around void at root

(W.Zhou, Long et al. 2007) reported that a crack was observed during tungsten inert gas welding of AZ91D related to the liquation of the second phase or low melting point precipitates in the heat affected zone (HAZ) or partial melting zone (PMZ). This type of crack is known as “liquation cracking” due to the existence of a low melting point for intermetallic compounds at grain boundaries of the HAZ and PMZ. These effects can greatly decrease the strength of the weld (W.Zhou, Long et al. 2007). However based on EDS analysis there was no segregation of Zn, Al and Mn in that area could be detected. Secondary phases of low melting intermetallic compounds consisting of Mg and Al or Zn did not precipitate near the crack areas. No finer grains were apparent at the open crack, which was likely observed in reference (W.Zhou, Long et al. 2007). Furthermore, no significant hardness was detected in this area. This further shows that precipitation of second phase low melting intermetallic compounds did not take place in the crack region.

However, a peak of O was apparent near the crack’s open surface. Although the surface of the thin sheet had been polished with SiC paper prior to welding, we believe that a thin oxide film probably still formed because magnesium is a very reactive metal. The crack probably initiated from the void at the root due to high stress concentrations, then propagated to the large elongated grain area along the thin oxide film.

During low scan speed welding, a wider area of large grains probably formed at the boundary of the fusion zone and base metal. This area was exposed to much lower temperature than the middle of the fusion zone; thus, oxide films were not properly broken or melted during welding. Furthermore, a low scan speed may result in high heat input, which consequently leads to higher stresses in the large grain area as the metal solidifies and contracts. Therefore, cracks could easily propagate throughout the oxide film area.

Higher scan speeds can reduce stress as well as leading to the formation of a wider fine equiaxed grain area. Subsequently, the large grain areas become much smaller, as shown in table 5.2. These fine equiaxed grains are less susceptible to cracking than larger ones because the stress is more evenly distributed among numerous grain boundaries.

### 5.3 Numerical simulation of lap fillet welding

This section present the simulation model of laser lap welding process utilize the efficient solution procedure of the finite element code ANSYS. The physical dimensions of the bond width, penetration depth and HAZ width were measured and compared with the prediction model.

#### 5.3.1 Geometrical model description

A moving, pulsed laser beam vertically radiated on the edge of upper sheet. The laser beam center located on edge of upper specimen and laser were scanned towards y direction. The pulse energy is sufficient to form a joint on the specimens. The dimensions of the thin sheets and heat source are shown in Fig. 5.7. The thin sheets with thickness of 0.3 mm is overlapped each other.

The following assumptions were made in the formulation of the finite element model:

1. The laser beam is incident vertically towards the surface of the workpiece. The heat or laser beam center is located at edge of upper specimen.
2. The laser beam spot diameter on surface of specimen is 0.4 mm. Half of the spot beam hit on upper sheet and other half on lower sheet.
3. The workpiece is initially at 20 °C. Both the laser beam and the coordinate mesh are fixed and the work pieces moves in the positive y-direction with a constant velocity,  $v$ .
4. All thermophysical are considered to be constant.
5. The absorption of laser is fixed at 18 %. This based on the experimental results which are around 18-20 %.

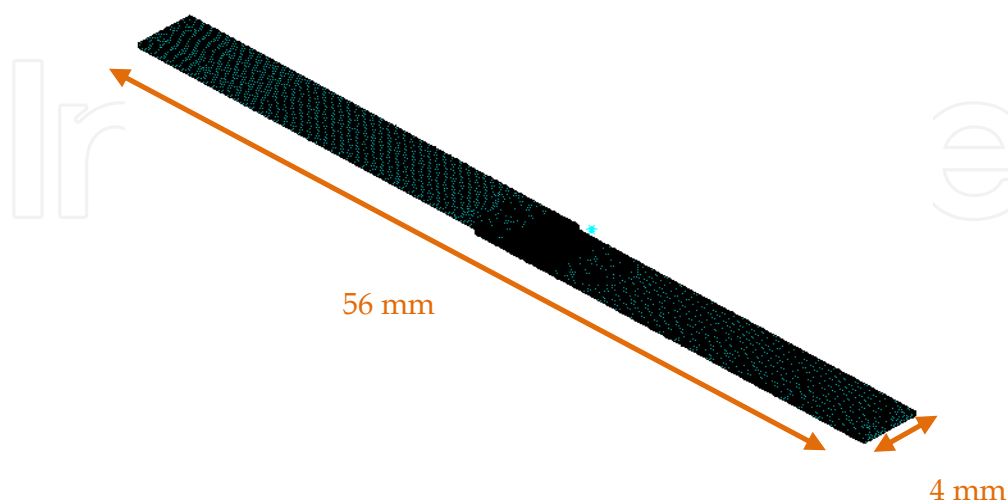


Fig. 5.7. Schematic drawing 3D geometrical model

6. The gap between the thin sheets is 30  $\mu\text{m}$  and is divided into two layers which thickness of 15  $\mu\text{m}$  each.
7. As pulsed laser welding involves very rapid melting and solidification, convective redistribution of heat within the weld pool is not a significant as it is in other processes where liquid pool is permanent. Convective flow of heat, therefore, is neglected.

The mesh structure of model is shown in Fig. 5.8. The mesh size is divided into 5 different zones. As the distance of specimens far away from weld area, the mesh becomes rougher. The finest mesh is defined at weld area where 84 mesh along the 4 mm width of specimen. Free mesh is defined at zone 1, while mapped mesh at zone 2, 3, 4 and 5. The thickness of mesh at zone 2 to zone 4 consists of 7 layers of one thin sheet, whereas, zone 1 only 1 layer. In this simulation, the pulse energy is fixed at 1.8 J, pulse duration 3.0 ms, repetition rate at 80 Hz. The simulation is done at three different scan speeds 250 mm/min, 350 mm/min and 450 mm/min. The simulation time was 0.53 s, 0.375 s and 0.2975 s for scan speed 250 mm/min, 350 mm/min and 450 mm/min, respectively.

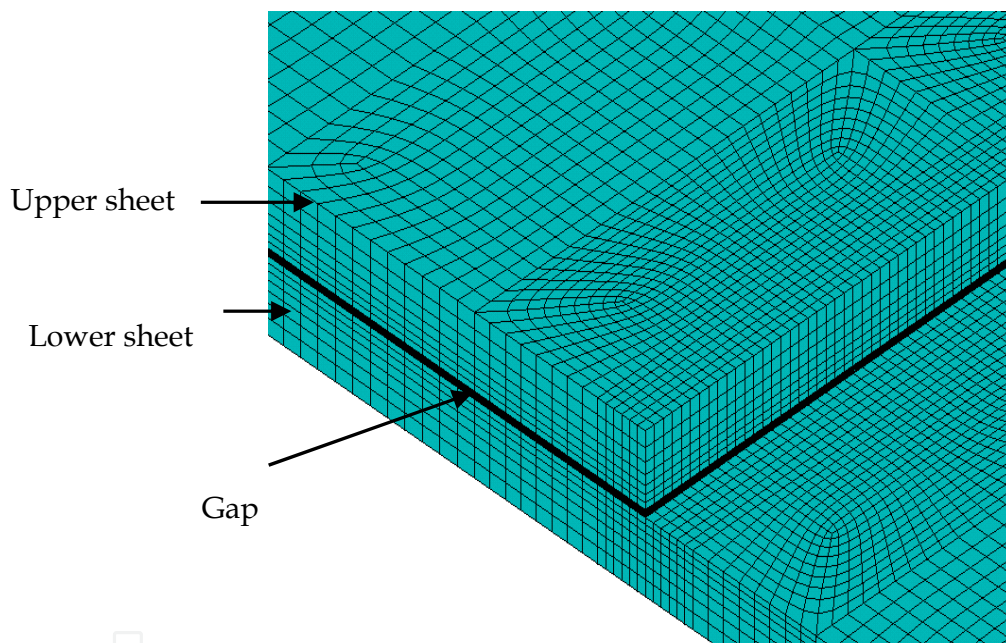


Fig. 5.8. Mesh structure at weld area

### 5.3.2 Numerical description

The temperature field caused by moving laser beam is transient in nature. Here, in order to simulate the process, a three-dimensional transient heat transfer model was constructed. The general three dimensional heat diffusion equations is of the form

$$\frac{\partial}{\partial x} \left( k_x \frac{\partial T}{\partial x} \right) + \frac{\partial}{\partial y} \left( k_y \frac{\partial T}{\partial y} \right) + \frac{\partial}{\partial z} \left( k_z \frac{\partial T}{\partial z} \right) + Q = \rho c \left( \frac{\partial T}{\partial t} - v \frac{\partial T}{\partial x} \right) \quad (5.1)$$

where,

$(x, y, z)$  = coordinate system attached to the heat source

$Q$  = power generation per unit volume ( $\text{W}/\text{m}^3$ )

- $k_x, k_y, k_z$  = thermal conductivity in the x, y, and z directions (W/mK)  
 $c$  = specific heat capacity (J/kgK)  
 $\rho$  = density (kg/m<sup>3</sup>)  
 $t$  = time (s)  
 $v$  = velocity of workpiece (m/s)

Laser heat input was on the surface as heat flux. Heat losses due to convection and radiation are very small (Yeung and P.H 1999) and hence also there were not considered in this analysis, as they make calculation non-linear, thus causing convergence problems and increasing computing time by a great amount.

The finite element code ANSYS provides the convenient means of numerically modeling pulsed laser welding. The solution technique is chosen depending on the type of problem. In the present case, the thermal history of lap fillet weld is required, so a transient thermal analysis must be performed. This requires an integration of the heat conduction equation with respect to time. In the finite element formulation, this equation can be written for each element as follow (Frewin and Scott 1999);

$$[C(T)\{\dot{T}\} + [K(T)\{T\} + \{V\} = \{Q(T)\} \quad (5.2)$$

where

- $[K]$  = conductivity matrix  
 $[C]$  = specific heat matrix  
 $\{T\}$  = vector or nodal temperature  
 $\{\dot{T}\}$  = vector of time derivative of  $\{T\}$   
 $\{V\}$  = velocity vector for the moving workpiece  
 $\{Q\}$  = nodal heat flow vector

This equation is simply the vector and matrix equivalent of Equation 4.4.

### 5.3.3 Numerical result and discussion

The predicted temperature distributions from numerical analysis at different scan speeds are shown in through Fig. 5.9. It is noted that the temperature distribution has a parabolic form, which is the consequence of the Gaussian energy profile. The maximum temperature is recorded at the central axis of laser beam. It is explained by the fact that the heat source is applied on the thin sheet surface at the edge of upper sheets.

The maximum temperature decreases as scan speed increases as a result of lower heat input. At scan speed of 250 mm/min the melt area are larger than scan speeds of 350 mm/min and 450 mm/min. It is also noted that the area of temperature between 500 °C until 575 °C becomes smaller as scan speed increases. This result because of heat input decreases as scan speed increases. From the results, it shows that the weld area slightly larger at starting (starting calculation time) and end point (end calculation time) of specimen compare with at the middle of the specimen. It shows similar tendency with the experimental results where wider weld zone and deeper penetration obtained at edge compare with at the middle of the specimen. This occurs because of lower heat concentration at middle than at the edge of

specimen. It is due to heat easily dissipated away as a result of high conductivity at the middle of specimen.

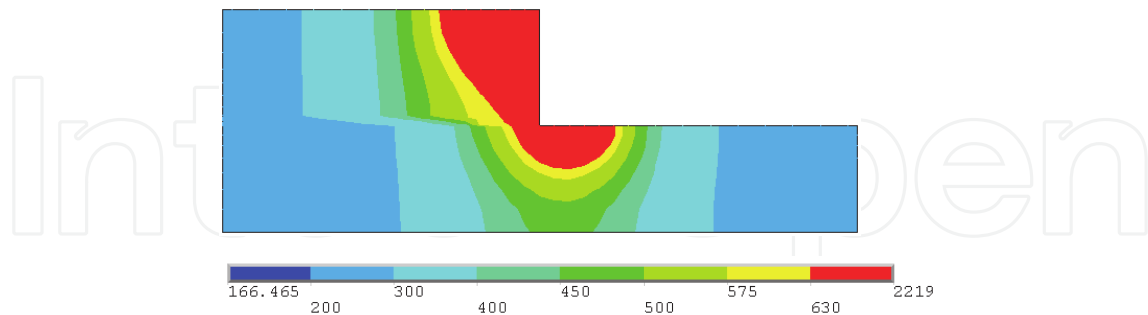


Fig. 5.9. Result of numerical simulation at scan speed 450 mm/min at  $t=0.2975s$

Fig. 5.10 shows the comparison between the numerical simulation result and cross section of experimental results. It shows that at higher scan speeds, the weld geometry between simulation and the experimental results are almost similar. Fig. 5.11 shows quantitative comparison between numerical and experimental results of fusion zone width, penetration depth and HAZ width at weld root. The fusion zone area is the area recorded temperature from melting point. Meanwhile, the HAZ width is measured at weld root with temperature between  $500^{\circ}C$  until  $575^{\circ}C$ . The range of HAZ temperature is based on grain growth studies of AZ31B (Mehtedi, Balloni et al. ; Ben-Artzy, Shtechman et al. 2000; Maryaa, Hector et al. 2006; Sun, Wu et al. 2009). The results of comparison between numerical calculation and experimental results show a reasonable agreement. At lowest scan speed of 250 mm/min, numerical result shows larger fusion width compare with experimental result. The different occurs because of larger defects (void and crack) at the weld root, and occurrence of severe undercut which result in smaller weld width of experimental result. The defects improve as scan speed increases. As a result, good agreement can be obtained at scan speed of 350 mm/min and 450 mm/min.

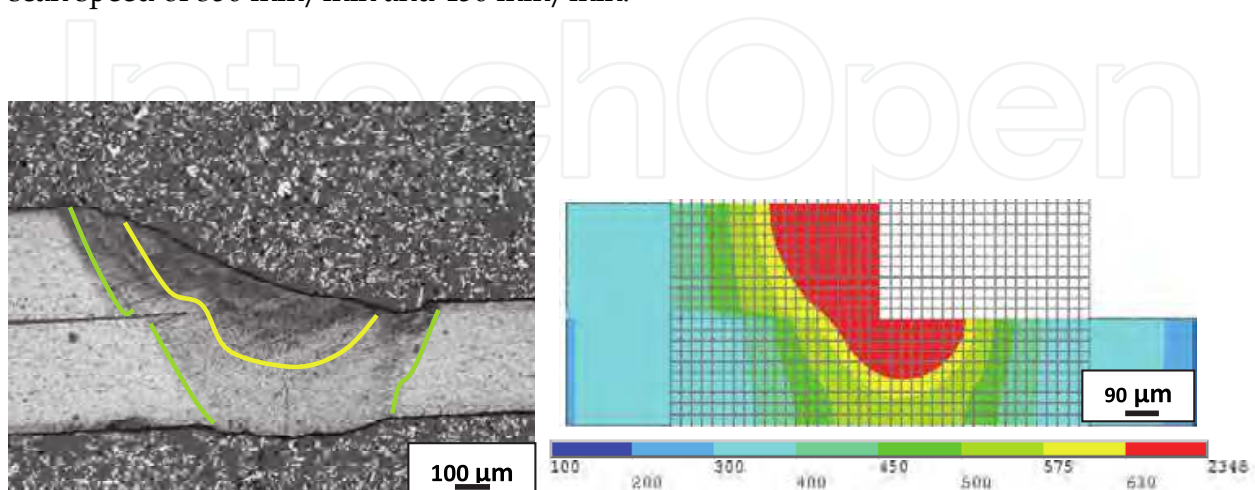


Fig. 5.10. Comparison between experimental and numerical result at scan speed 250 mm/min

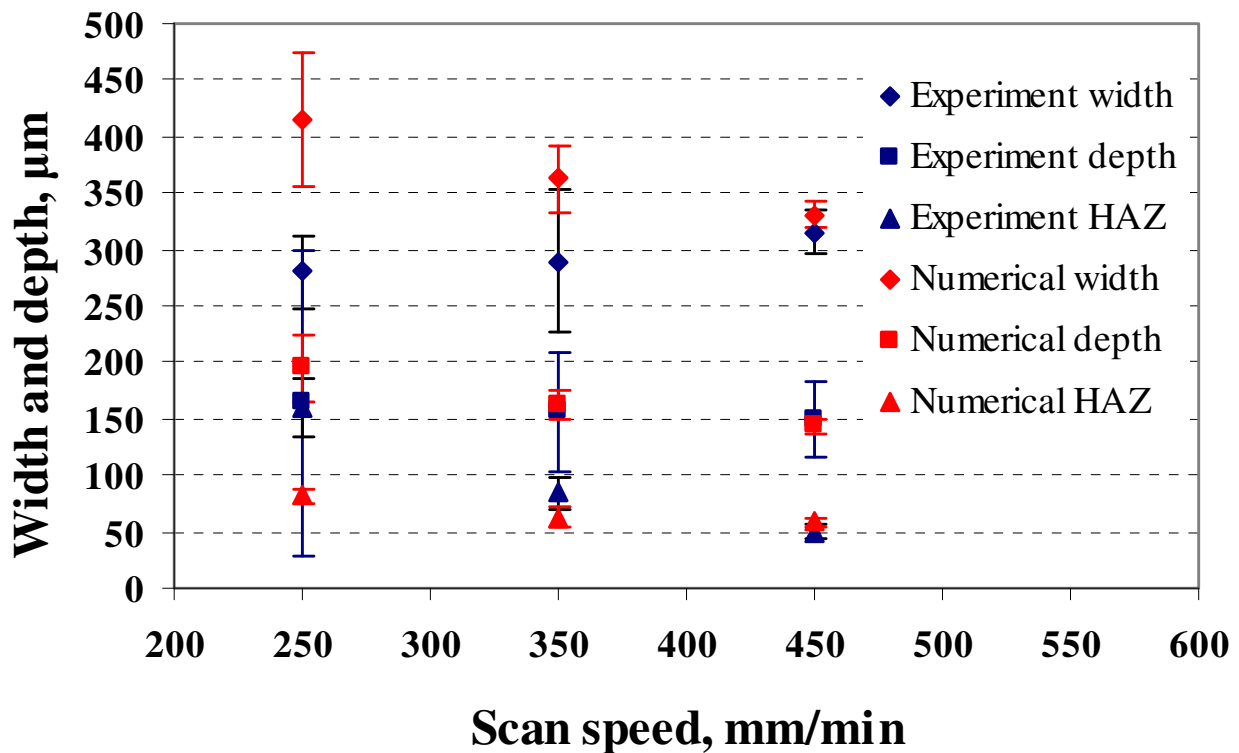


Fig. 5.11. Comparison of weld geometry and HAZ width between experimental and numerical results at different scan speeds

## 6. Conclusion

We investigated the influences of welding parameters, such as beam center location, laser scan speed and gap size, on weldability in the context of lap fillet welding of AZ31B magnesium alloys with a thickness of 0.3 mm with a pulsed Nd:YAG laser. The following conclusions can be drawn from this work:

For bead on plate (BOP) welding undercut, cracks and pores can be greatly reduced when the process parameters were properly chosen to weld bead on the AZ31B magnesium alloy sheet in the Nd:YAG laser welding system. The depth of penetration decreases as focus point located on surface of thin sheet magnesium alloys. The defects such as undercut, cracks and pores are significantly reduced as pulse energy at 1.8 J, repetition rate at 80 Hz, pulse duration 3.0 ms and scan speed range from 300 to 500 mm/min.

The gap width exerts a major influence on the occurrence of joints and defects, such as cracks and voids, between the two sheets. A gap width of less than 35  $\mu\text{m}$  significantly reduces the number of cracks and voids and also increases the penetration depth and bond width.

Voids and discontinuities at the root occurred because of lack of fusion. A narrow gap oxide layer on the lower surface acted as a heat barrier to prevent melting of the lower sheet. High scan speeds significantly improved the number of voids and discontinuities at the root. Cracks at the weld originated from voids at the root, which propagated in a transgranular manner within the large grain area. No segregation of Al, Mn and Zn occurred at the crack

opening, whereas a high content of oxide may have caused the crack/discontinuity. Higher scan speeds significantly reduced the number of defects because of the narrower large grain area and the wider fine grain area.

Lap fillet welding of the thin sheet produced a weld bead width of less than 1 mm, with no melt-through and good weld bead appearance, when the beam center location was on the edge of the upper specimen and when we used scan speeds of 350 to 450 mm/min. Under the optimized conditions, a large fine grain size area can be obtained from the top to the middle of the weld bead, and the HAZ becomes very narrow.

The weld geometry (weld width, depth and HAZ width) of numerical simulation results show reasonable agreement with experimental results at high scan speed of 350 mm/min and 450 mm/min.

## 7. References

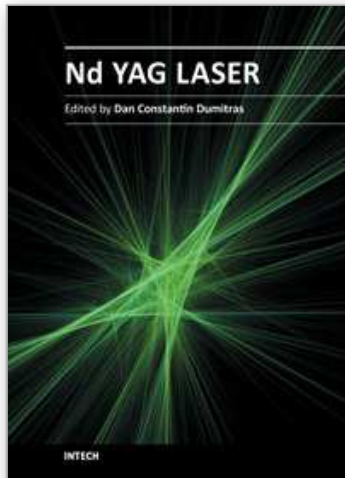
- Aghios, E., B. Bronfiu, et al. (2001). "The role of the magnesium industry in protecting the environment." *Journal of Materials Processing Technology* 117: 381-385.
- Ben-Artzy, A., A. Shtechman, et al. (2000). "Deformation characteristics of wrought magnesium alloys AZ31, ZK60." *Magnesium Technology*: 363-374.
- Cao, X., M. Jahazi, et al. (2006). "A review of laser welding techniques for magnesium alloys." *Journal of Materials Processing Technology* 171: 188-204.
- Cao, X., M. Jahazi, et al. (2006). "A review of laser welding techniques for magnesium alloys." *Journals of Materials Processing Technology* 171: 188-204.
- Costaa, A. P., L. s. Quintinoa, et al. (2003). "Laser beam welding hard metals to steel." *Journal of Materials Processing Technology* 141: 163-173.
- Czerwinski, F. (2002). "The oxidation behavior of an AZ91D magnesium alloy at high temperatures." *Acta Materialia* 50: 2639-2654.
- Duley, W. W. (1998). *Laser welding*, A Wiley-Interscience publication.
- Duley, W. W. (1999). *Laser Welding*, John Wiley & Sons, Inc.
- Frewin, M. R. and D. A. Scott (1999). "Finite element model of pulsed laser welding." *Welding research supplement*: 15s-21s.
- G. Ben-Hamu, D. E., and C. E Cross, Th. Bollinghaus, , . (2007). "The relation between microstructure and corrosion behavior of GTA welded AZ31B magnesium sheet." *Materials Science and Engineering A* 452-453: 210-218.
- G.Rihar and M.Uran (2006). "Lack of fusion-Characterisation of indications." *Welding in the world issue* 1/2 50(1/2): 35-39.
- Haferkamp, H., A. Ostendorf, et al. (2003). *Laser beam welding of magnesium alloys a process at the threshold to the industrial manufacturing*. International Conference on Leading Edge Manufacturing in 21st Century: 891-896.
- Ion, J. C. (2005). *Laser Processing of Engineering Materials*, Elsevier.
- Ishak, M. (2010). *Study on Lap Fillet Welding of AZ31B Magnesium Thin Sheets using Pulsed Nd:YAG Laser*. Graduate School of Science and Engineering, Ibaraki University, Japan. Phd thesis.

- Ishak, M., K. Yamasaki, et al. (2009). "Lap fillet welding of thin sheet AZ31magnesium alloy with pulsed Nd:YAG laser." *Journal of Solid Mechanics and Materials Engineering* 3(9): 1045-1056.
- Leong, K. H., K. R. Sabo, et al. (1999). "Laser beam welding of 5182 Aluminum alloy sheet." *J. Laser Applications* 11(3): 109-118.
- Liming Liu and Changfu Dong (2006). "Gas tungsten-arc filler welding of AZ31 magnesium alloy." *Materials letters* 60: 2194-2197.
- Maryaa, M., L. G. Hector, et al. (2006). "Microstructural effects of AZ31 magnesium alloy on its tensile deformation and failure behaviors." *Materials Science and Engineering, A418*: 341-356.
- Mehtedi, M. E., L. Balloni, et al. "Comparative study of high temperature workability of ZM21 and AZ31 magnesium alloys." *Metallurgical science and technology*: 23-30.
- Moon Jonghyun, K. S., Mizutani Masami, and Matsunawa Akira (2002). "Lap welding characteristics of thin sheet metals with combined laser beams of different length (In Japanese)." *Japan welding society* 20: 468-476.
- Nobuyuki, A., T. Masahiro, et al. (2002). "Welding of Aluminum Alloy with High Power Direct Diode Laser, ." *Trans. JWRI* 31(2): 157-163.
- Quan, Y. J., Z. H. Chen, et al. (2008). "Effects of heat input on microstructure and tensile properties of laser welded magnesium alloy AZ31." *Mater. Charact.* 59(10): 1491-1497.
- Sun, P.-h., H.-y. Wu, et al. (2009). *Deformation Characteristics of Fine-grained Magnesium Alloy AZ31B Thin Sheet during Fast Gas Blow Forming*. Proceedings of the International MultiConference of Engineers and Computer Scientists 2009 (IMECS 2009).
- Toshikatsu Asahina, H. T., Hitaka Itoh and Shigekazu Taguchi (2005). *Some characteristics of pulsed YAG laser welds of Magnesium Alloys*. Nihon University research report 38, Nihon University.
- Ukita, S., T. Akamatsu, et al. (1993). "The welding conditions of very thin aluminum sheet of high welding." *Japan welding society* 11: 361-364.
- W.Zhou, T. Z. Long, et al. (2007). "Hot cracking in tungsten inert gas welding of magnesium alloy AZ91D." *Mat. Sci. and Tech.* 23 (11): 1294-1299.
- Y.Quan, S. C., Z. Yu, X.S. Gong, M.Li, (2008). "Characteristics of laser welded wrought Mg-Al-Mn alloy." *Materials Characterisation* 59: 1799-1804.
- Yamauchi, N., Y. Inaba, et al. (1982). "Formation mechanism of lack of fusion in MAG welding." *Japan welding society (in Japanese)* 51(10): 843-849.
- Yeung, K. S. and T. P.H (1999). "Transient thermal analysis of spot welding electrodes" *Welding Journal* 78(1): 1s-6s.
- Z. Barsoum and A. Lundback (2009). "Simplified FE welding simulation of fillet welds-3D effects on the formation residual stresses." *Eng. Fail. Anal.* 16(7): 2281-2289.
- Zhao, H. and T. Debroy (2001). "Pore Formation During Laser Beam Welding Of Die-Cast Magnesium Alloy AM60B –Mechanism And Remedy." *Weld. Research Supp*: 204s-210s.

Zhu, J., L. Li, et al. (2005). "CO<sub>2</sub> and diode laser welding of AZ31 magnesium alloy." *Applied Surface Science* 247 pp. 300-306.

IntechOpen

IntechOpen



## **Nd YAG Laser**

Edited by Dr. Dan C. Dumitras

ISBN 978-953-51-0105-5

Hard cover, 318 pages

**Publisher** InTech

**Published online** 09, March, 2012

**Published in print edition** March, 2012

Discovered almost fifty years ago at Bell Labs (1964), the Nd:YAG laser has undergone an enormous evolution in the years, being now widely used in both basic research and technological applications. Nd:YAG Laser covers a wide range of topics, from new systems (diode pumping, short pulse generation) and components (a new semiorganic nonlinear crystal) to applications in material processing (coating, welding, polishing, drilling, processing of metallic thin films), medicine (treatment, drug administration) and other various fields (semiconductor nanotechnology, plasma spectroscopy, laser induced breakdown spectroscopy).

### **How to reference**

In order to correctly reference this scholarly work, feel free to copy and paste the following:

Mahadzir Ishak, Kazuhiko Yamasaki and Katsuhiro Maekawa (2012). Laser Welding of Thin Sheet Magnesium Alloys, Nd YAG Laser, Dr. Dan C. Dumitras (Ed.), ISBN: 978-953-51-0105-5, InTech, Available from: <http://www.intechopen.com/books/nd-yag-laser/laser-welding-of-thin-sheet-magnesium-alloys>

**INTECH**  
open science | open minds

### **InTech Europe**

University Campus STeP Ri  
Slavka Krautzeka 83/A  
51000 Rijeka, Croatia  
Phone: +385 (51) 770 447  
Fax: +385 (51) 686 166  
[www.intechopen.com](http://www.intechopen.com)

### **InTech China**

Unit 405, Office Block, Hotel Equatorial Shanghai  
No.65, Yan An Road (West), Shanghai, 200040, China  
中国上海市延安西路65号上海国际贵都大饭店办公楼405单元  
Phone: +86-21-62489820  
Fax: +86-21-62489821

© 2012 The Author(s). Licensee IntechOpen. This is an open access article distributed under the terms of the [Creative Commons Attribution 3.0 License](#), which permits unrestricted use, distribution, and reproduction in any medium, provided the original work is properly cited.

IntechOpen

IntechOpen